1994

Mammogram segmentation using fuzzy pyramid linking

Milorad Neskovic
Lehigh University

AUTHOR:

Neskovic, Milorad

TITLE:

Mammogram Segmentation Using Fuzzy Pyramid Linking

DATE: October 9, 1994

MAMMOGRAM SEGMENTATION USING FUZZY PYRAMID LINKING

by

Milorad Neskovic

A Thesis

Presented to the Graduate Committee

of Lehigh University

in Candidacy for the Degree of

Master of Science

in

Department of Electrical Engineering and Computer Science

Lehigh University

1994

This thesis is accepted in partial fulfillment of the requirements for the degree of Master of Science.

9/28/94
(Date)

Prof. Dragana Brzakovic
Thesis Advisor

Prof. Alastair McAulay
Chairman, Department of EECS

Abstract

In this theses a method for multiresolution image segmentation is implemented and tested. The essence of the method is hierarchical region growing and pyramidal multiresolution image representation. The relationship between pixels on different pyramid levels is modeled by fuzzy membership function. The selection of the parameters of the fuzzy membership function allows for fine–tuning the method to specific segmentation objectives. The method is tested on recognition of microcalcifications and nodules in mammographic images using normal mammograms with superimposed synthetic objects and mammograms containing cancer.

Acknowledgments

The author wishes to express his appreciation to his advisor, Prof. Dragana Brzakovic, for invaluable support, advice, and unwavering patience and encouragement that she has given to him throughout his masters program. It is hard to put down in words the value of the privilege of working with her.

Special thanks are extended to the Lehigh University, Bethlehem, and the Department of Electrical Engineering and Computer Science for providing an excellent graduate study program and research environment.

The author deeply owns to his friend Nenad Vujovic for invaluable support, advice and help throughout his undergraduate and graduate studies. Many thanks to his friend Predrag Bakic for his valuable help and encouragement. Finally, and most importantly, the author would like to thank his parents for their sturdy motivation and strong support.

Contents

List of Tables

List of Figures

Chapter 1

Introduction

Breast cancer is currently the second cause (next to lung cancer) of cancer-related mortality in the female population in the USA [1],[2]. It is estimated that 150,000 new cases of breast cancer were detected in 1990 and 44,000 deaths were caused by it in the same year [1]. It is also predicted that these numbers will increase in the future [3]. Early detection of breast cancer is the key to successful treatment and reduction of mortality. Consequently, routine mammograms are recommended for a large percentage of the female population as the most reliable detection method. On average, a mammogram can detect breast cancer two years before it is palpable. Studies have shown that properly administered mammograms can reduce the overall mortality from breast cancer in specific groups of the population by 30%. Consequently, NCI has chosen breast cancer screening as one of its high priorities for the year 2000. One of the major obstacles towards achieving this goal is high cost of the procedure. Part of this cost is associated with mammogram reading, which is performed by highly skilled experts. Considering that, typically, there are four mammograms associated with an individual, a viable means of reducing the cost is

to replace a part of the manual readings by automated, computer-based mammogram analysis. In addition, automation offers consistency in performance since it is not subject to fatigue.

Automated mammogram analysis has attracted considerable attention of researchers over the past two decades [4]. Due to complexity of the problem, researchers have considered specific subproblems. Some of them attempt to automatically detect and classify abnormal regions of the breast, such as circumscribed or stellate lesions. The others attempt to detect and classify microcalcification, which are present in $30 - 50\%$ of breast carcinomas [5]. The proposed solutions may be classified in two major categories: computer detection systems (CDS) and a computer classification systems (CCS). Differences between them are as follows. CDS attempt to find areas of abnormality in mammograms and report their location. CCS have a broader scope; they not only have the role of reporting the location of abnormalities, but also classifying those abnormalities into malignant or benign [4].

This work concentrates on the problem of mammogram segmentation and detection of abnormalities and thus is classified as a CDS.

Segmentation of a mammogram should output two types of regions: potentially cancerous regions and normal regions. Variations within the limits of normality of highly textured breast tissue pose an obstacle in achieving this objective. Cancerous changes may be very subtle, of low contrast, and with hazy borders. Consequently, cancerous changes are frequently less visible than variations in the normal tissue.

Highly textured backgrounds in mammograms dictate selection of image segmentation methods that are successful in dealing with texture regions. Multi-resolution pyramid based image segmentation [6], [7] is chosen as the basis of the work described in this thesis. The concept of pyramid based segmentation was proposed earlier [8] for detection of fine details in complex texture backgrounds and is based

on fuzzy set theory. The method was proved successful in segmenting low resolution mammograms containing large tumors, as described in [9]. In this thesis, fuzzy pyramid linking was modified to detect subtle intensity changes and small detail (microcalcifications).

The thesis is organized as follows. Chapter 2 is a review of recent work in the area of computer mammography. Chapter 3 describes the fuzzy pyramid linking method. Modifications of the method and parameter selection for segmentation of mammograms are described in Chapter 4. In Chapter 5 performance evaluation of the fuzzy pyramid linking method is presented.

Chapter 2

Review of Related Work in Computer Aided Mammography

Recently, automated mammogram analysis has attracted a number of researchers the field of computer image processing. Due to complexity of the problem, specific subproblems are considered. One group of researchers is concerned with detection of abnormal regions in a breast such as lesions and masses; another group is concerned with detection of microcalcification. Both of the groups are involved in the design of CDSs. In contrast, a number of researchers have made an effort to classify abnormal areas as malignant or benign, and they are involved in building a CCSs. The difference between CDSs and CCSs is that former report if there are abnormalities in mammograms and where they are located, while the later in addition determines if the abnormalities are malignant or benign. Stewart *et al.* [4] argued that CDSs are more likely to influence medical care in the near future.

2.1 Computer Analysis of Mammograms Containing Masses

In this section we review systems that detect and classify masses in mammographic images in chronological order. The earliest work involving computers in mammogram analysis was done by Winsberg *et al.* in 1967 [10] who tried to locate breast lesions by comparison of the left and the right breasts. Mammograms were digitized to a pixel dimension of 0.14×0.14 mm and 8 gray levels. A digitized mammogram was divided into 64 small regions (windows) to allow comparison between the same regions in the left and right breast. Each region was characterized by four vectors derived from the light intensities in the region. Area, distribution, contiguity, and uniformity vectors were calculated for each grey level. The vector sets for the two breasts were then combined and differences were analyzed resulting in detection of abnormal areas. The method was able to detect lesions in selected cases.

Ackerman *et al.* [11] in 1973 published a paper describing 36 mammogram properties of lesions in benign and malignant breast disease cases. A list of properties was compiled, in order of the importance, by a radiologist. The most important properties were: mass diameter, percentage of peripheral fat, mass border and the number of suspicious areas. This properties were later used by other researchers [12], [13] to incorporate some form of knowledge in their systems.

Kimme *et al.* [12] described first fully–automatic detection and classification system in 1975. The procedure is applied on the breast tissue of the mammogram only and as a first step the white halo is detected. Second, both left and right breasts were partitioned into rectangles of fixed dimensions of breast tissue so that regions of similar tissue could be compared with one another. Then, ten statistics features

of the regions were calculated. Finally, the differences between the features of corresponding rectangles in two breasts were analyzed. They started with resolution of 200 dots per inch (*dpi*) and then reduced it twice to lower the storage requirements.

Hand *et al.* [13] in 1979 described a procedure for locating suspicious areas in a mammogram. Original image of 1400×1029 pixels was reduced by replacing each 10×10 window, called Primary Resolution Cell (PRC), with 14 parameters describing the PRC. These parameters measured intensity, roughness, and directionality within the PRC. The breast boundary was chosen by setting thresholds for three intensities and directional parameters in a PRC. Parameters were then combined to measure 'circle–likeness' and 'star–likeness' of objects in the PRC. A combination of intensity, circle and star–likeness were used to generate the 'activity' parameter, one for each breast. Then subtracting the activity parameter of one of the breasts from that of the other defines the suspicious parameters. These parameters were run through the low–pass filter and thresholded. Corresponding areas were marked as suspicious.

Similar approach was taken by Semmlow *et al.* [14] who further extended the Hand *et al.* work to classification. They used 16–level gray scale images and extracted PRC. Four parameters were calculated from PRCs: one represented intensity, one roughness, and other two directionality. The outline of the breast was determined by first locating the nipple using a spatial filter and then applying the Sobel's edge detector. Suspicious areas were detected similarly as described in [13] by using activity and suspicious parameters. Feature extraction was employed and cluster analysis was performed to facilitate classification.

Gale *et al.* [15] investigated important mammographic signs of malignancy. The objective was to discriminate between malignant and benign disease. Study showed that 12 out of the initial 39 signs were important in discrimination. This conclusion was important, because it allowed for simplification of the classification rule.

Brzakovic *et al.* [9] introduced a system for automatic detection and analysis of benign and malignant carcinomas in mammograms. Described procedure split processing in two stages. First, homogeneous regions were distinguished from the background by using fuzzy pyramid linking and thresholding. The second stage classified the segmented objects into three classes: benign, malignant, and normal. Classification was performed by using Bayes classifiers and deterministic rules applied in a hierarchical structure. The structure was organized in such a way that simplest measurements (such as size and shape compactness) were situated at the top and the procedure continued only if a reliable classification could not be made with these measurements. The complexity of measurements increased at lower levels.

2.2 Computer Analysis of Mammograms with Microcalcifications

In 1978 Hoyer and Spiesberger [16] described a system which attempted to detect masses as well as calcifications.They worked with fairly large resolution of $1000dpi$. Program first found the outline of the breast considering the grey level differences between pixels in both the horizontal and vertical directions. When these differences were larger than the threshold, the pixels were marked as the breast outline. Next, extraction of texture features was performed for windows of the specified sizes and features were compared. Calcifications were detected by investigation of the central pixel in a 19×19 window (covering $0.5 \times 0.5mm$) which was moved over image. If the central pixel was a local bright spot then the pixel was marked as a location of a possible calcification. After completition the initial marking of locations, the test for compactness and brightness was run in order to reduce the number of potential

calcifications leaving only true calcifications.

Some authors were more interested in computer aided enhancement than actual classification. Chan *et al.* [17] obtained a "difference image" by subtracting a signal–suppressed version of the original image from the enhanced version. In order to get a signal enhanced image, they applied a matching filter to the image. The signal suppressed image was generated by applying a median filter. The difference image was then thresholded in two different modes: global, where the gray levels above the threshold value were retained, and local, in which the local statistics within a square window of 51×51 pixels were used to determine a dynamic threshold value. At the end signal extraction was achieved through the use of a boundary detection procedure and the area thresholding criterion derived from known characteristics of micro-calcifications.

Olsen *et al.* [18] studied the image properties of breast micro-calcifications and tried to discriminate benign from malignant calcifications. They digitized 48 mammograms to a pixel dimension of 0.21×0.21 mm and at 256 grey levels. First, an analysis program provided general image statistics such as histogram, intensity averages, medians and standard deviations, and then another program located calcifications. On the basis of coordinate locations the following features were identified: calcification size, calcification intensity, average grey level of regions surrounding the calcification, cluster size, etc.

One of the recent attempts to detect micro-calcification clusters was done by Bankman *et al.* [19]. Their work is based on consideration that the mammogram images are 3–D landscapes where the brightness of the mammogram is represented by the elevation of the landscape. Because micro-calcifications are relatively brighter than their immediate surroundings, they appear as prominent peaks that stand out with respect to the local surrounding. The algorithm first generates the contour

map of the image with iso–intensity contours obtained by thresholding. In the contour map, each peak is represented by a nested set of contours. Contours whose areas are too large to be parts of micro-calcification are disregarded. Each peak is characterized by a sequence of contour areas. Then, final decision is made after extracting and classifying 5 features from the area sequence of peaks: departure, prominence, steepness, distinctness, and compactness. For the discrimination between micro-calcifications the Bayesian classifier was used.

Chapter 3

Texture Image Segmentation

This chapter describes the fuzzy pyramid linking method. First, the notion of pyramids and pyramid linking is described in Sections 3.1.1 and 3.1.2, respectively. Next, the details of fuzzy pyramid linking and the role of specific parameters are discussed in Section 3.2.

3.1 Pyramid-based Image Segmentation

The segmentation methods employing pyramids are in essence hierarchical region growing methods that use efficient multi-resolution image representation. In the following section common characteristics of methods that fall into this category was reviewed.

3.1.1 Image Pyramids

An image pyramid is a convenient and efficient representation of an image at multiple resolutions. It is created by using the original image I_0 of dimensions $2^n \times 2^n$ as the base of the pyramid. Each subsequent level of the pyramid, $I_1 \ldots I_n$, is a

square array which is half the dimension of its predecessor. These arrays are lower resolution representations of the original image. The top level I_n of the pyramid is a 1×1 array. An element (node) of the array I_l ($l > 0$) is obtained by a weighted averaging of the I_{l-1} nodes within a $k \times k$ neighborhood. A pyramid is created using a specific weighting scheme. Subsequently, a pyramid may be redefined using an algorithm. This section discusses pyramid creation, and Section 3.1.2 reviews algorithms for redefining pyramid structures.

The selection of different weighting schemes for pyramid creation yields different types of pyramids. A convenient approach to choosing weights is to use a Gaussian weighted averaging technique. The image pyramid thus created is known as a Gaussian pyramid [20]. The Gaussian pyramid was utilized in this work and the following discussion is limited to this pyramid; more general discussion on pyramids can be found in [21].

The creation of each level, I_l, $l = 1, 2, ..., n$, in the Gaussian pyramid is obtained by convolving the image one level below, I_{l-1}, with a 4×4 Gaussian mask $w(p, q)$; therefore, an element at location (i, j) at level l is created from elements at level $l - 1$ using

$$I_l(i,j) = \sum_{p=-2}^{2} \sum_{q=-2}^{2} w(p,q) I_{l-1}(2i+p-\frac{p}{2|p|}+\frac{1}{2}, 2j+q+\frac{1}{2}-\frac{q}{2|q|}) \quad for\ p, q \neq 0. \quad (3.1)$$

Our implementation is based on the idea of the Hierarchical Discrete Correlation (HDC) [22]. Among various implementations of HDC involving odd or even neighborhoods the even neighborhood size was chosen. The selection was made based on the fact that the even neighborhood: (i) requires fewer calculations (computations are carried out over neighborhood 4×4, rather than 5×5), and (ii) offers advantages in linking procedures. The reduced size pyramid is generated by retaining every second pixel at each of the levels. The relationships between pixels at different levels of the pyramid for 1-D case are shown in Figure 3.1. The extension to a 2-D case

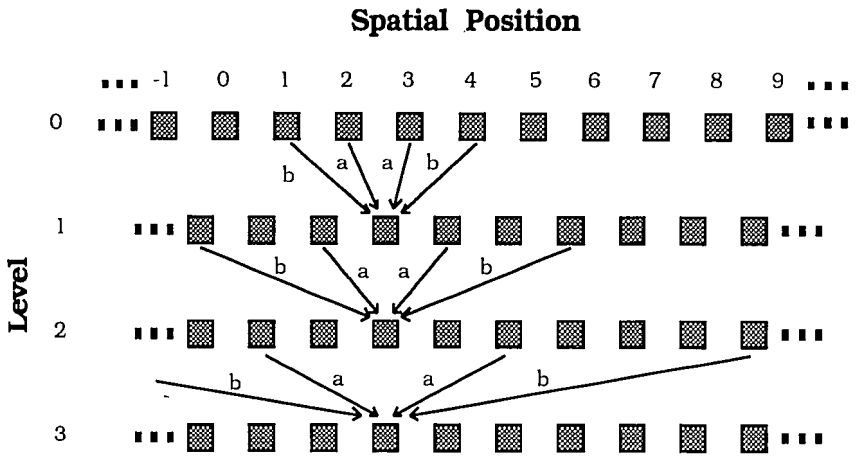

Figure 3.1: Even Hierarchical Discrete Correlation in a 1-D case. Relationships between successive levels of pyramid. Values a and b denote weights of the Gaussian mask.

is straightforward. It should be noted that the Gaussian mask must be separable, normalized, and symmetric [20].

3.1.2 Pyramid Linking

Linking is the process by which nodes belonging to a given level of the pyramid are connected with nodes at adjacent levels, i.e., links establish relationships between pixels at different resolutions. Links are first used to redefine the pyramid iteratively and then to segment the image by replacing the nodes at level $l-1$ by the nodes at level l.

Since each Gaussian pyramid level is created by convolving the 4×4 weight mask with the preceding level of the pyramid, there exists a predetermined spatial relationship between nodes at two adjacent levels. From Equation (1) it follows that each node at level l, $l > 0$, has a 4×4 array of candidate child nodes at level $l-1$. Conversely, for each node at level l, $l < n-1$, there exists a 2×2 array of candidate

parent nodes at level $l + 1$. The links are established for all child nodes in the pyramid starting with the base of the pyramid and using a chosen link algorithm. The pyramid is redefined iteratively and new links are determined. The pyramid structure converges once the links within the pyramid stabilize.

Image segmentation can be achieved upon convergence by mapping the lower resolution image at the apex of the pyramid onto the original image at the base of the pyramid by following the linking paths through the intermediate levels. This form of segmentation by hierarchical region growing results in a number of regions equal to or less than the number of nodes at the apex of the pyramid, provided that there are no constraints limiting the propagation of the apex nodes to the base of the pyramid.

Various algorithms have been proposed for linking nodes at adjacent levels of the pyramid. Some of the proposed algorithms link a child node to the parent node that is the most similar based on a chosen property, e.g., intensity. These algorithms are frequently referred to as hard linking. In this thesis, a different algorithm is proposed. Difference is that a child node is linked to all four candidate parent nodes. This algorithm differs from hard linking in that it allows connections between intensities that differ significantly, and the strength of the link is a function of the absolute difference between the value of a child node and its candidate parent node. By choosing different functions determining the strength of the link, various levels of detail can be extracted from texture images. It should be noted that this approach allows obtaining results identical to hard pyramid linking when choosing a particular type of linking function and/or its parameters.

3.2 Fuzzy Pyramid Linking

The linking algorithm used in this work is detailed in Section 3.2.1, followed by a discussion on the selection of the linking function (Section 3.2.2) and its parameters (Section 3.2.3).

3.2.1 Algorithm for Redefining Pyramid and Segmentation

The algorithm described in this section was proposed by Sufi [23]. The algorithm uses the following variables are defined for the linking and ensuing iterative pyramid redefining process:

- $t_l(i,j)$: the *local image property* (in this paper intensity);
- $p_l(i,j)$: the *pointer* to the node's parent one level above having the maximum link strength, hereafter referred to as *the maximum link*;
- $s_l(i,j)$: the *strength value of the link* between the parent and the child nodes.

The iterations proceed in the following manner:

1. For level $l = 0$ set

$$s_0(i,j) = 1 \quad \text{and } t_0(i,j) = I_0(i,j).$$

2. For each level l from 1 to $n-1$ set

$$s_l(i,j) = \sum_{i'j'} s_{l-1}(i',j')\phi_{i,j,i',j'},$$

where $\phi_{i,j,i',j'}$ denotes the strength of the link between the node (i,j) at level l and its child (i',j') at level $l-1$,

and

$$t_l(i,j) = \sum_{i'j'} t_{l-1}(i',j')\phi_{i,j,i',j'},$$

with summations performed over all children of the node.

3. For each node at level l, for $0 \leq l < n-2$, the pointer $p_l(i,j)$ points to the parent node at level $l+1$ that has the maximum link strength among the four candidate parent nodes. If two or more parents have the same link strength, a link is chosen randomly; however, if either link existed in the previous iteration, the link remains unchanged.

4. Once the links have propagated to the top of the pyramid the value of every node, except those at level 0, is recomputed in the following manner:

$$I_l(i,j) = t_l(i,j)/s_l(i,j) \quad for\ s_l(i,j) > 0.$$

5. If no link is reassigned during the current iteration, it is assumed that a steady state has been reached. If any number of links have been reassigned during the current iteration, the procedure is repeated starting from Step 2.

Upon reaching steady state, image segmentation is achieved in one top-down pass beginning from level $n-1$. In this pass, a child node at level l is replaced by the parent node pointed to by $p_l(i,j)$. The proposed algorithm limits the propagation of the links for specific nodes by requiring that the links between the child and parent nodes (pointed by $p_l(i,j)$) exceed a specified threshold τ.

3.2.2 Modeling Strength of the Link

The choice of the function ϕ, representing the strength of the link, determines the flexibility of the pyramid segmentation. Various monotonically decreasing functions

were considered by Sufi [23] for modeling the strength of the link, including the linear-like, sigmoid-like, and fuzzy membership functions. Characteristics of the class of images to be segmented combined with the objectives of segmentation determine the best type of function. Considering Fisher ratios and false detections, the fuzzy membership function was found to be the most flexible of the three [23]. The linking algorithm employing this function is appropriately called *fuzzy pyramid linking.*

The fuzzy membership function is widely used in various applications based on the fuzzy set theory [24]. In these applications the objective is to establish imprecise relationships between objects and concepts, as is the case in this work. Therefore, the strength of the link between nodes (i,j) and (i',j') is modeled by

$$\phi_{i,j,i',j'}(u;\alpha,\beta,\gamma) = 1 - S(u;\alpha,\beta,\gamma), \tag{3.2}$$

where

$$S(u;\alpha,\beta,\gamma) = \begin{cases} 0 & \text{for } u \le \alpha \\ 2\left(\frac{u-\alpha}{\gamma-\alpha}\right)^2 & \text{for } \alpha \le u \le \beta \\ 1 - 2\left(\frac{u-\gamma}{\gamma-\alpha}\right)^2 & \text{for } \beta \le u \le \gamma \\ 1 & \text{for } u \ge \gamma \end{cases} \tag{3.3}$$

and $u = |I_l(i,j) - I_{l-1}(i',j')|$. The parameters α and γ determine the shape of the function, and $\beta = \frac{\alpha+\gamma}{2}$. Values of $\phi_{i,j,i',j'}$ range between 0 and 1, and the assignment of specific values is determined by the selection of α and γ. The roles of these two parameters are discussed in the next section.

The function $\phi_{i,j,i',j'}$, described by Equations (2) and (3), makes the proposed pyramid linking method a special case of fuzzy isodata clustering [23]. Consequently, based on the convergence of fuzzy isodata clustering [25], the proposed pyramid linking is convergent [23]. (The relationship between pyramid linking and isodata clustering is discussed by Kasif and Rosenfeld [26].)

3.2.3 Parameter Selection: General Concerns

The discussion in this section is divided into two parts. First, the selection of the parameters for the fuzzy membership function is discussed. These parameters include α and γ, both of which determine how the pyramid is redefined in the iterative process. Next, we discuss parameter selection for segmentation (that follows the iterative process). The segmentation parameters include the threshold value τ and the level of pyramid from which segmentation starts. The following discussion concentrates on general considerations, while the specific selection of parameters for segmenting mammograms is described in Sections 4.1-4.3.

Parameters for defining the pyramid

Parameters α and γ determine how intensities are weighted when generating the next level of the pyramid. Specifically, parameter α determines the difference between pixel values at adjacent levels below which the link strength is 1; while γ is the difference above which the link strength is 0. Combined they determine how much child nodes that differ from the parent node in the previous iteration contribute to the value of that parent node in the next iteration. Physically, it makes sense to assign relatively small integer values to α, e.g., $\alpha = 0, 1, 2, ...5$, and considerably larger integer values to γ. The general considerations in choosing the values for these parameters are as follows.

Parameter α. Since parameter α allows two pixel values I_l and I_{l-1} (at levels l and $l-1$, respectively) to be considered as having the same value if $|I_l - I_{l-1}| \leq \alpha$, the selection of this parameter is dictated by (i) expected noise level and (ii) minimum contrast, μ_c, to be detected. Generally, parameter α should satisfy $\alpha << \mu_c$ and it should be larger than the expected variations due to noise. The two considerations

may be conflicting. However, noise effects are of lesser importance due to the fact that through multiresolution processing the noise effects are reduced. Therefore, minimum contrast is the dominating criterion for selecting α. It should be noted that the selection of α in general does not impact the results significantly. We have obtained consistent results by employing $0 \leq \alpha \leq 15$ for different classes of images, including mammograms [8],[9].

Parameter γ. The impact of this parameter is significant as it has two effects: (i) it determines the intensity difference $|I_l - I_{l-1}|$ beyond which two pixels are unrelated, and (ii) it determines the weight values for parent (I_l) and child (I_{l-1}) nodes satisfying $\alpha < |I_l - I_{l-1}| < \gamma$. If γ is chosen close to α, function ϕ [Equation (2)] approaches a step function and the proposed algorithm approaches hard pyramid linking. This selection is appropriate when sharp edges are present and accurate segmentation is the objective. On the other hand, when objects are of low contrast, it is necessary to choose larger values for γ. It should be noted that γ can be chosen larger than the number of intensities in an image, thus implying that all intensities are related and allowing all child nodes to contribute on an almost equal basis to the parent node. The specific value for γ should be chosen based on the distribution of intensities in an image (image histogram) and the objective of segmentation, i.e., expected variations within statistically homogeneous regions.

Segmentation parameters

The segmentation results using the fuzzy pyramid structure are strongly influenced by the level from which segmentation starts and the threshold value τ. The impact of the two is as follows.

Pyramid Level. The level of the pyramid from which the segmentation starts determines the maximum number of regions that can be detected in an image when

replacing child nodes with the parent nodes, starting from the top of the pyramid and going to the bottom and assuming that the maximum links exceed the threshold value. Fuzzy pyramid linking allows for the creation of a potentially larger number of regions since some pixels may retain their original values (and are not replaced) due to thresholding.

Threshold value τ. This parameter is the most critical and decides whether a child node can be replaced by a parent node in the segmentation procedure. Therefore, it determines the final number of regions in the segmented image since the maximum links whose values are below the threshold value do not propagate down to the base of the pyramid. Generally, $0 \leq \tau \leq 1$, and high values of the maximum links are associated with homogeneous regions, while low values appear around edges. Choosing a small τ allows practically all links to propagate, thus generating few regions in a segmented image. On the other hand, large values of τ do not allow most of the maximum links to propagate, and the segmented image resembles the low-pass filtered original image. The range of the maximum links in an image is determined by the image intensities and the selection of γ. Therefore, it is appropriate to choose threshold value adaptively after studying the histogram of the maximum links for a specific image and taking into consideration the objectives of image segmentation.

Using the guidelines described in this section, we have adapted the fuzzy pyramid linking algorithm to mammogram segmentation. The selection of specific parameters and utilization of the algorithm is described in the next chapter.

Chapter 4

Mammogram Segmentation

This chapter is divided into three parts. First, Section 4.1 discusses the characteristics of mammogram images and the appropriate selection of parameters α and γ. Sections 4.2 and 4.3 detail the utilization of fuzzy pyramid linking for detecting microcalcifications and nodules, respectively. These sections discuss the strategies employed, the appropriate pyramid level to start segmentation, and the selection of parameter τ. The segmentation procedures used for extracting microcalcifications and nodules are summarized in Table 1.

4.1 Selection of Fuzzy Membership Function Parameters

Generally, useful parts of mammogram images (breast region) are highly textured and contain a narrow range of gray levels; e.g., when digitized to 256 gray levels their histograms contain about 100 different intensities and typically the histograms are unimodal. The presence of cancerous changes is statistically insignificant except

in cases of advanced cancer, which are of little interest in massive screening of mammograms. Noise arising from digitization is relatively low and of less concern than highly textured and varying characteristics of the normal breast tissue.

The objective of segmentation is to detect objects of low contrast (nodules) that vary in shape and size, and very small objects of somewhat higher contrast (microcalcifications). Taking into account these objectives, the characteristics of mammograms, and the general discussion in Section 3.2.3, $\alpha = 1$ is chosen. This selection is primarily motivated by our desire to detect objects of low contrast. As already mentioned, the results are stable for a range of values of α, and we have experimented with $0 \leq \alpha \leq 15$ without noticing significant difference in the results. The selection of low values of α has little impact on digitization noise, which is taken care of by the very nature of multiresolution processing.

Considering that the range of gray levels is relatively low and that relationships between all intensities exist, $\gamma = 100$ is chosen, thus allowing all intensities to be weighted similarly and creating a truly fuzzy relationship between pixels at different pyramid levels. All images discussed in this thesis were processed using the same values of parameters α and γ. Therefore, it is implicitly assumed that each of the images is subject to low noise level, the objects of interest are of low contrast and practically all intensities in an image are related. If either of these assumptions are violated it is necessary to choose different parameters using guidelines in Section 3.2.3.

Since there are only a few sharp intensity transitions in mammograms, my selection of values for parameters α and γ results in the maximum links close to 1 for most of the pixels. The only exceptions are very small objects, such as microcalcifications, which have somewhat smaller maximum links. It should be noted that all of the processed mammograms that contain no microcalcifications have high maximum links. Two typical histograms of the maximum links are shown, together with

Table 4.1: Selection of parameters for extracting microcalcifications and nodules

objective	# of images used	links[1]	α	γ	τ	level[2]
microcalcifications	2	NP	1.	100.	ϕ^{min}[3]	4×4
		NP	1.	100.	$\phi^{min} + \delta$[4]	4×4
small nodules	2	NP	1.	100.	ϕ_1[5]	4×4
		NP	1.	100.	ϕ_2[6]	4×4
large nodules	1	P	1.	100.	0.	$2^n/\sqrt{A}$[7]

[1] NP-utilize only nodes whose maximum links do not propagate from the top of the pyramid; P-utilize only nodes whose maximum links propagate from the top of the pyramid.
[2] Level is chosen based on corresponding image size (actual level depends on the initial size of the image).
[3] Choose ϕ^{min} such that at $K = 40$ nodes have links smaller than ϕ^{min}.
[4] Choose δ such that $2K$ nodes have links smaller than $\phi^{min} + \delta$.
[5] Choose ϕ_1 such that $K = 2A$ nodes have links smaller than ϕ_1
(A is the expected maximum area of the objects of interest).
[6] Choose ϕ_2 such that $2K = 4A$ nodes have links smaller than ϕ_1 (A is the expected maximum area of the objects of interest).
[7] the chosen level is of size $2^n/\sqrt{A} \times 2^n/\sqrt{A}$; $2^n \times 2^n$ is the image size.

corresponding images, in Figure 4.1. The difference between the two images is that the image in Figure 4.1(a) contains more texture variation, in comparison to image in Figure 4.1(b).

4.2 Detection of Microcalcifications Using Fuzzy Pyramid Linking

Individual microcalcifications are typically small, sometimes only one pixel in size, and vary slightly in intensity from the surrounding area. Therefore, the microcalcifications are associated with pyramid nodes that have relatively small maximum links close to the base of the pyramid. When choosing low values for threshold τ, with selection of parameters α and γ described in Section 4.1, most of the child nodes will be replaced by the parent nodes, thus generating large uniform regions in the segmented images. Only pixels corresponding to edges and small objects, such as individual microcalcifications, retain their original intensities in the segmented image. The two groups of pixels can be easily differentiated since the groups corresponding to edge pixels increase in size when τ is increased, while small objects retain their shape and size. Consequently, microcalcifications are detected in the following three steps.

1. Upon pyramid convergence, generate histogram of the maximum links $\phi_{max}(i, j, i', j')$, and determine the minimum value of the maximum links ϕ^{min}. It should be noted that it is necessary to quantize values of ϕ_{max}. A slightly larger value is chosen for ϕ^{min} if the number of nodes associated with the true minimum is very small. The value ϕ^{min} is chosen such that at least $K = 40$ nodes have $\phi_{max} \leq \phi^{min}$.

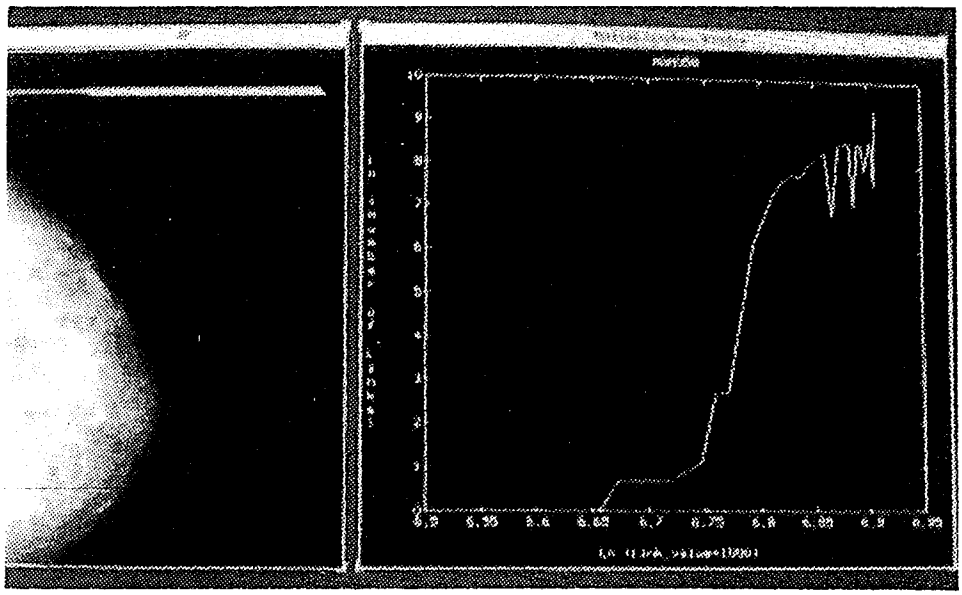

(a)

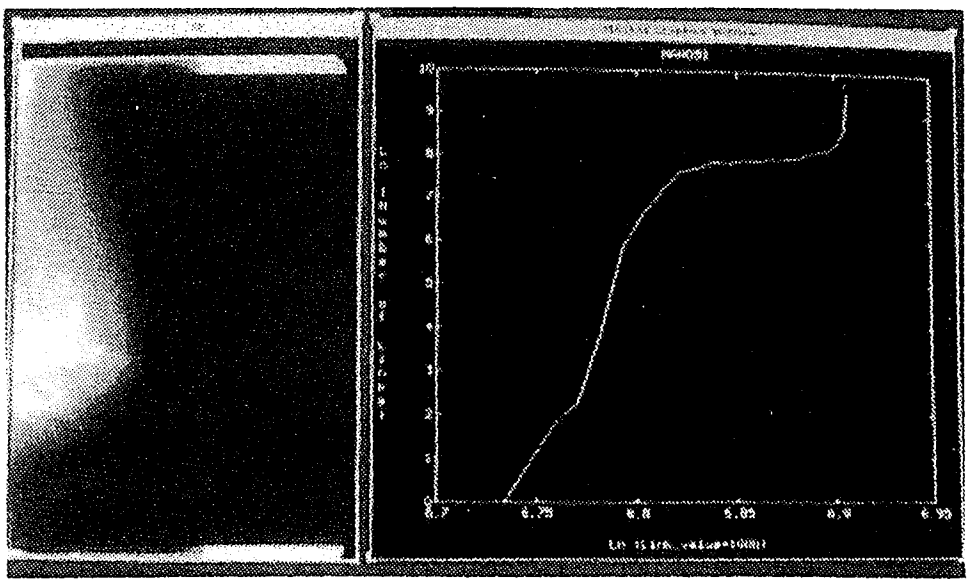

(b)

Figure 4.1: Examples of typical histograms of maximum links (shown on logarithmic scale): (a) textured mammogram and its maximum link histogram, and (b) relatively uniform mammogram and its maximum link histogram.

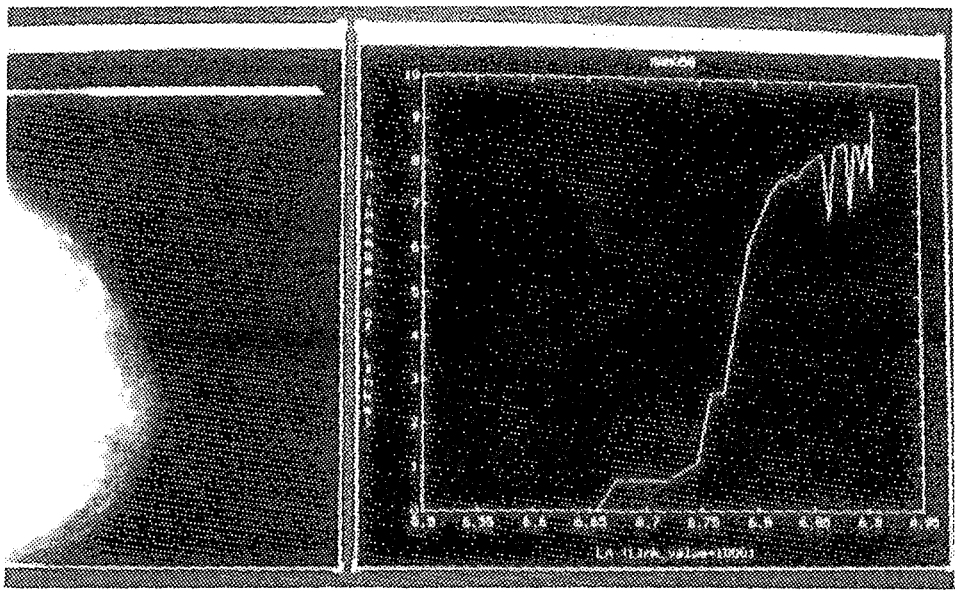

(a)

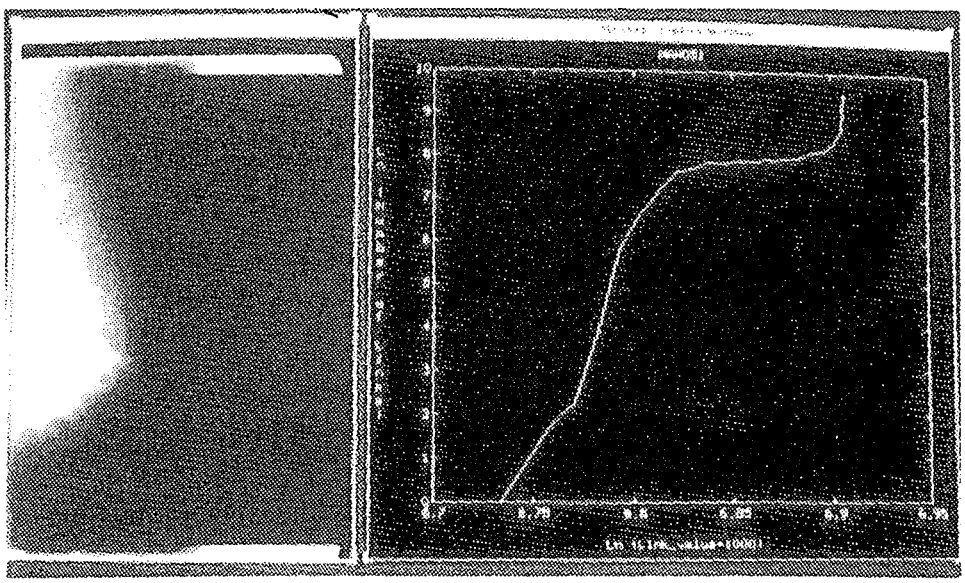

(b)

Figure 4.1: Examples of typical histograms of maximum links (shown on logarithmic scale): (a) textured mammogram and its maximum link histogram, and (b) relatively uniform mammogram and its maximum link histogram.

2. Generate segmented image, I_{s0}, using $\tau_0 = \phi^{min}$. Next, generate segmented image, I_{s1}, using $\tau_1 = \phi^{min} + \delta$, where δ is chosen such that at least $2K$ nodes have $\phi_{max} \leq \tau_1$.

3. Compare I_{s0} and I_{s1} and determine if there are pixel groupings in two images that have not changed size. Extract these pixels and generate segmented image containing potential microcalcifications. Retain in segmented image only the pixels whose maximum links did not allow them to be replaced by pixels at the very top of the pyramid.

Considering that a mammogram may contain nodules or other bright regions, segmentation is started at the pyramid level that has size 4×4, thus allowing the existence of 16 homogeneous regions. The choice of parameter K in Step 1 is determined by the expected number of pixels corresponding to microcalcifications, and K should be larger than that number. The selection of δ in Step 2 should be such that I_{s1} contains observable differences relative to I_{s0}. If $\tau_0 = \tau_1$, i.e., more than $2K$ pixels are associated with ϕ^{min}, the next value of ϕ_{max} is chosen for τ_1. Neither of the values K or δ is critical for the success of the method; however, the above guidelines keep the algorithm in Step 3 simple. The evaluation of the performance of this method on mammograms containing microcalcifications as well as normal mammograms containing synthetically superimposed microcalcifications is described and quantitatively summarized in Chapter 5. The evaluation incorporates both the ability to detect microcalcifications as well as false alarms.

4.3 Detection of Nodules Using Fuzzy Pyramid Linking

Nodules, benign and malignant, are generally characterized by higher intensities (relatively to the surrounding tissue) and are relatively homogeneous, at least in the center. However, they may have ill-defined boundaries. In contrast to microcalcifications, the nodules are relatively large. Depending on the size of the nodules we propose two approaches. The first is used for the detection of small nodules and uses the procedure described in Section 4.2. The only difference is that in Steps 1 and 2 the threshold values τ_0 and τ_1 are chosen differently, based on the expected maximum size of the object, A. Value τ_0 is chosen such that $K = 2A$ nodes have the maximum links smaller than this value. The threshold value τ_1 is chosen such that $2K$ nodes have the maximum links smaller than τ_1.

A different version of fuzzy pyramid linking is used for the detection of larger objects. There are two basic differences, the level from which the segmentation starts and the selection of parameter τ. The first is dictated by the size of the objects to be detected. The smaller the objects, the lower the level of pyramid is chosen; practically, this means that it is appropriate to choose the level of pyramid which allows the object "to be seen". Since objective is to detect homogeneous regions, it is necessary that all links propagate through the pyramid. The image of interest, in contrast to microcalcification detection where we are interested only in pixels whose links did not propagate from the top of the pyramid, is the image where all pixels were replaced by the pixels at the top of the pyramid (i.e., the level from which the segmentation has started). The nodules are extracted in the following three steps.

1. Choose $\tau < \phi^{min}$ and perform segmentation as described in Section 4.2.

2. Linearly scale and threshold the result. (In this work the thresholding algorithm described in [27] is used.)

3. Check the size, intensity characteristics, and shape of each remaining object. Extract objects that are less than the specified size (in our case 1/10 of the total image size), have higher values than the image mean, and have a relatively circular shape (we have used the measure of compactness). These objects are potential nodules.

The simple reasoning is employed in the third step; more sophisticated considerations, like complex shape analysis, can eliminate most of the false alarms.

Chapter 5

Performance Evaluation

Performance evaluations were carried out using: (i) synthetically generated objects superimposed on normal mammograms and (ii) digitized mammogram images. The experiments with synthetically generated objects were carried out on two different backgrounds (normal mammograms), and the each object was placed at five or more locations in the image, and the results were averaged for different locations. Total of 89 real mammograms were used for the evaluation; 50 of the mammograms were normal, 27 contained microcalcifications, and 12 contained nodules. All images were processed by subdividing a mammogram into non-overlapping windows of size 256×256 and integrating the individual results. The specific experiments and results are described in the following. First, Section 5.1 describes synthetic object generation, and Sections 5.2 and 5.3 summarize the results for detection of microcalcifications and nodules, respectively.

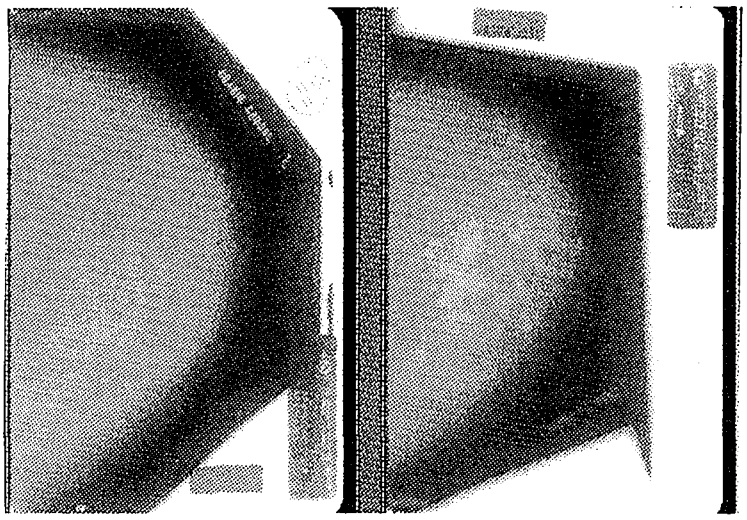

(a) (b)

Figure 5.1: Two normal mammograms that were used as the background for superimposing synthetic objects: (a) low textured background, (b) highly textured background.

5.1 Synthetic Image Generation

The superposition of synthetically generated objects on real mammograms provides for an objective study of capabilities of the method regarding contrast, size, and shape of objects. The error estimation in this case is accurate since the truth images are known precisely.

Normal mammograms of varying texture complexity were used as the background for the study. The complete sets of experiments were carried out using two mammograms, shown in Figure 5.1, as the background. These two mammograms were chosen because they represent extremes in complexity of generic textures in the given sample set of images. The mammogram shown in Figure 5.1(a) is characterized by limited variation in intensity, while the mammogram shown in Figure 5.1(b) is highly textured and a more challenging background for the tests.

Two sets of experiments were carried out. The first set pertains to establishing

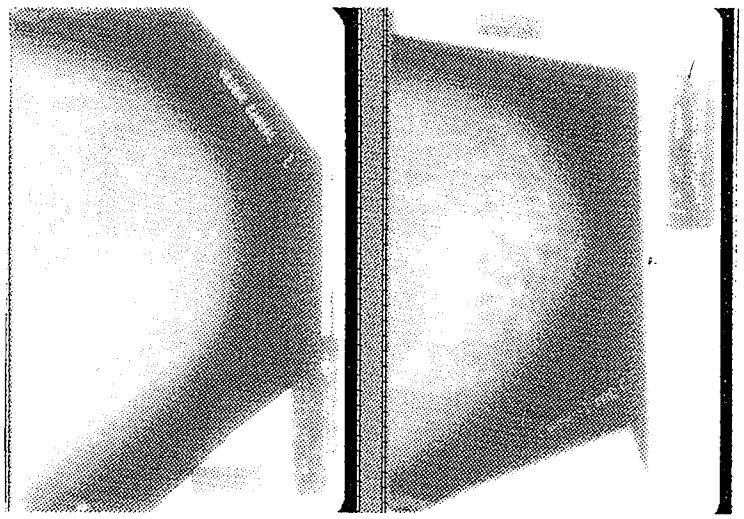

Figure 5.1: Two normal mammograms that were used as the background for superimposing synthetic objects: (a) low textured background, (b) highly textured background.

5.1 Synthetic Image Generation

The superposition of synthetically generated objects on real mammograms provides for an objective study of capabilities of the method regarding contrast, size, and shape of objects. The error estimation in this case is accurate since the truth images are known precisely.

Normal mammograms of varying texture complexity were used as the background for the study. The complete sets of experiments were carried out using two mammograms, shown in Figure 5.1, as the background. These two mammograms were chosen because they represent extremes in complexity of generic textures in the given sample set of images. The mammogram shown in Figure 5.1(a) is characterized by limited variation in intensity, while the mammogram shown in Figure 5.1(b) is highly textured and a more challenging background for the tests.

Two sets of experiments were carried out. The first set pertains to establishing

the capability of the proposed method to detect microcalcification, and the objective of the second set was to evaluate the performance when detecting larger low contrast objects, simulating nodules (benign and malignant). In both cases the objects were modeled in the same way, and by using different placement rules and specific parameters different classes of objects were generated.

Object Model

An object in all experiments was modeled by an ellipse with a specified major axis, minor axis, and the angle ω between the major axis and the x-axis (horizontal axis). By varying the ratio of the two axes the objects could vary from circular to very elongated ellipses of varying ω centered at the same point. A star-like structure encountered in some nodules, was generated by a number of elongated ellipses of varying ω. Microcalcifications were modeled by a pattern of small circular objects placed in a spiral fashion around a specified center (the number of objects was varied).

Object Edges

In order to allow natural variation in edge location, edges of each object were deformed using a random number generator (and a specified seed); pixels were either removed or added to the individual edge locations depending on if the number returned by the random number generator was odd or even. By repeatedly performing edge deformation, an object was deformed as desired.

Edge Profiles

Generally, objects of interest in mammograms do not have sharp edges and blend with the surrounding area. Therefore, we have chosen to model object edges using the ramp edge model, in contrast to the step edge model. The ramp edge model allows a gradual transition of intensities and a blending of objects and backgrounds.

An object was assigned a chosen intensity, i, and the object edge profiles were changed into ramps of specified profile. The center of the ramp was placed on the

physical edge of the object, and the intensities gradually changed starting from the inside of the object. (Clearly, there is a relationship between object size (in particular minor axis) and possible width of the ramp.) Finally, the object is superimposed on the chosen background. It should be noted that the true edge locations remain unchanged relative to the step edges since the ramp is centered at the step edge. Therefore, the truth images correspond to the step edge model. An object may be subjected to Gaussian noise of specified mean and standard deviation prior to being superimposed onto the background image.

By changing the intensity, i, incrementally, identical images with varying object contrast were generated for the purpose of studying the sensitivity of the proposed method to contrast. By keeping the intensity the same and changing the values of the major and minor axes, the sensitivity of the proposed method to object shape was studied. In both studies the objects were placed at various locations in the same image, and the errors were averaged for different placements in order to countereffect the impact of specific background intensities.

5.2 Detection of Microcalcifications

It is well established that microcalcifications are one of the earliest signs of potential cancerous changes in breast tissue [28]. Physically, microcalcifications have dimensions between .1-1. mm (in mammograms), implying that they are guaranteed to be correctly digitized when using a resolution of at least $50\mu m$. Mammograms digitized at lower resolutions may still show the presence of microcalcifications; however, the contrast between the microcalcifications and the surrounding tissue is much lower, and in some cases, depending on resolution, the microcalcifications are blended into surrounding tissue (through digitization) and are not detectable in the digitized images. The results obtained when applying the fuzzy pyramid linking

algorithm (Section 4.2) to synthetic microcalcifications and real microcalcifications are described in the following.

Synthetic microcalcifications

A limited number of available mammograms containing microcalcifications has motivated us to perform these experiments. In addition, some of the available mammograms were of lower resolution than required; therefore, we could not draw any reliable conclusions based on them. The primary objective of our experiments was to determine the lowest contrast for which the method was able to correctly detect the synthetic objects. The experiments were carried out by generating clusters of objects ranging individually in diameter from 1 to 3 pixels and placing identical clusters over a normal mammogram at different locations. Different locations were chosen in order to avoid the impact of neighboring intensities that may make detection easier in some cases. The results were averaged for different locations. The contrast of a cluster of objects was varied relative to the mean of the image region in predetermined steps.

The performance of the method varied with the complexity of the texture background. The method was able to correctly detect objects placed on the background in Figure 5.1(b) up to a contrast difference of 15 (between the region mean and the objects). By further lowering the contrast, the number of pixels that the method could not detect increased, and finally at contrast difference 10 only 60% of pixels were correctly detected. The average standard deviation of the background was in this case 9.5. In the case of the background shown in Figure 5.1(a), which is less textured, the method was able to detect the synthetic objects correctly for contrasts up to 10. By decreasing contrast to 9, the number of correctly detected pixels was reduced to 80%. The average standard deviation of the background was in this case 5.3. In either of the cases, the method did not detect any false positives. Two examples of superimposed objects, the truth images, and the obtained results are

shown in Figure 5.2.

The superposition of synthetic objects allowed evaluating the method's capabilities to detect objects that are small and have specific contrast; however, the background in the experiments differs from the case of detecting microcalcifications in high resolution mammograms in that the latter is expected to show more variations in the intensities of the normal tissue. However, the expected variations are relatively small and, as discussed in Section 3.2.3, are unlikely to significantly impact the results.

Real Microcalcifications

The performance of the method was evaluated on two sets of images. The first set contained 17 mammograms containing microcalcifications and 50 normal mammograms. This set was supplied by the University of South Florida and was accompanied by the corresponding truth images. These images were of considerably lower resolution than required by the sampling theorem and physical size of individual microcalcifications. The results on these images are as follows:

- The method has detected the presence of microcalcifications in 13 images (out of 17) in the same regions as in the accompanying truth images.
- The method has detected fewer individual microcalcifications than the truth images point at in the cluster regions. (On average, one out of four individual microcalcifications indicated in the truth images was missed.)
- No false positives were detected in any of the normal mammograms.
- No microcalcifications were detected in 4 images (out of 17) labelled as containing microcalcifications, and in another image (out of the remaining 13) no microcalcifications were detected in one of the regions pointed at by the truth image.

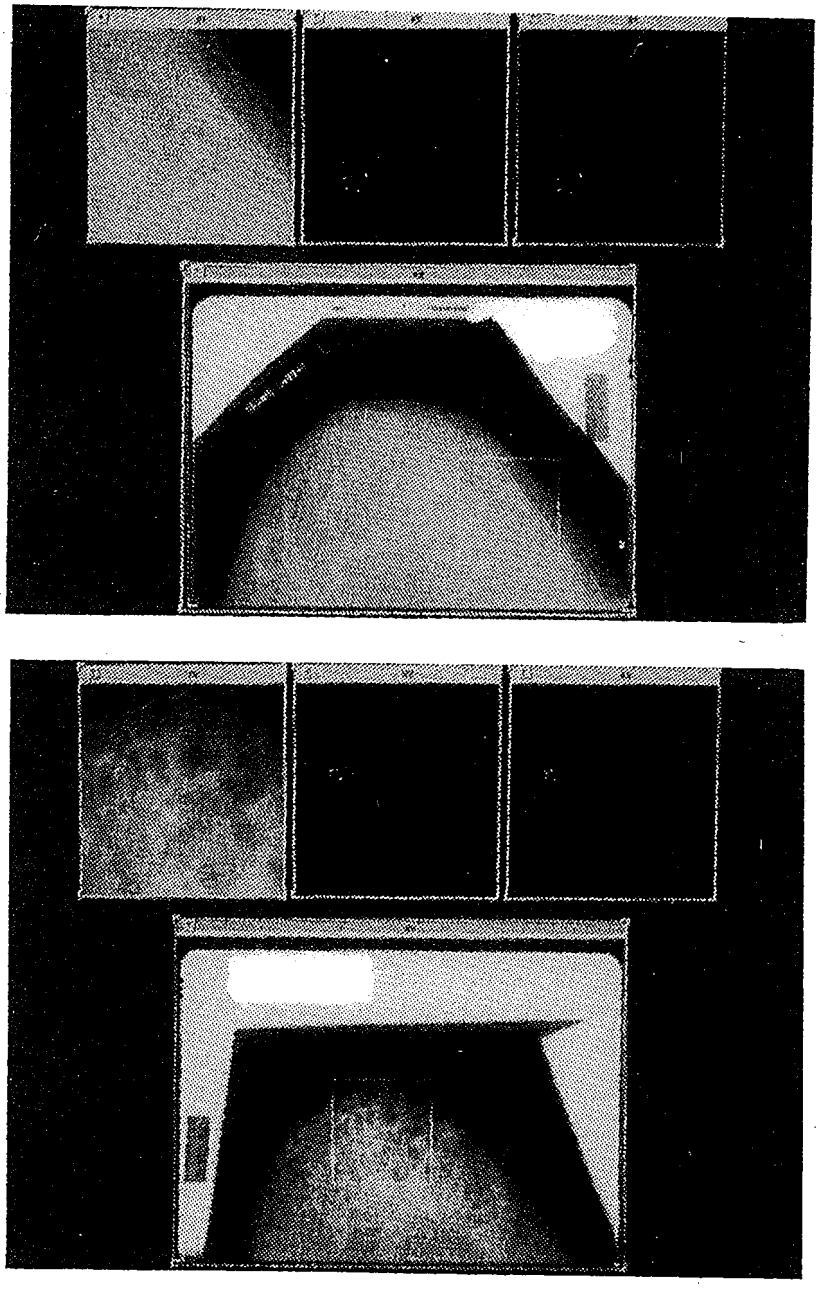

Figure 5.2: Two examples of superimposed synthetic microcalcifications on normal mammograms. The regions where the objects were superimposed are shown enlarged, together with the truth images and the segmentation results (left to right).

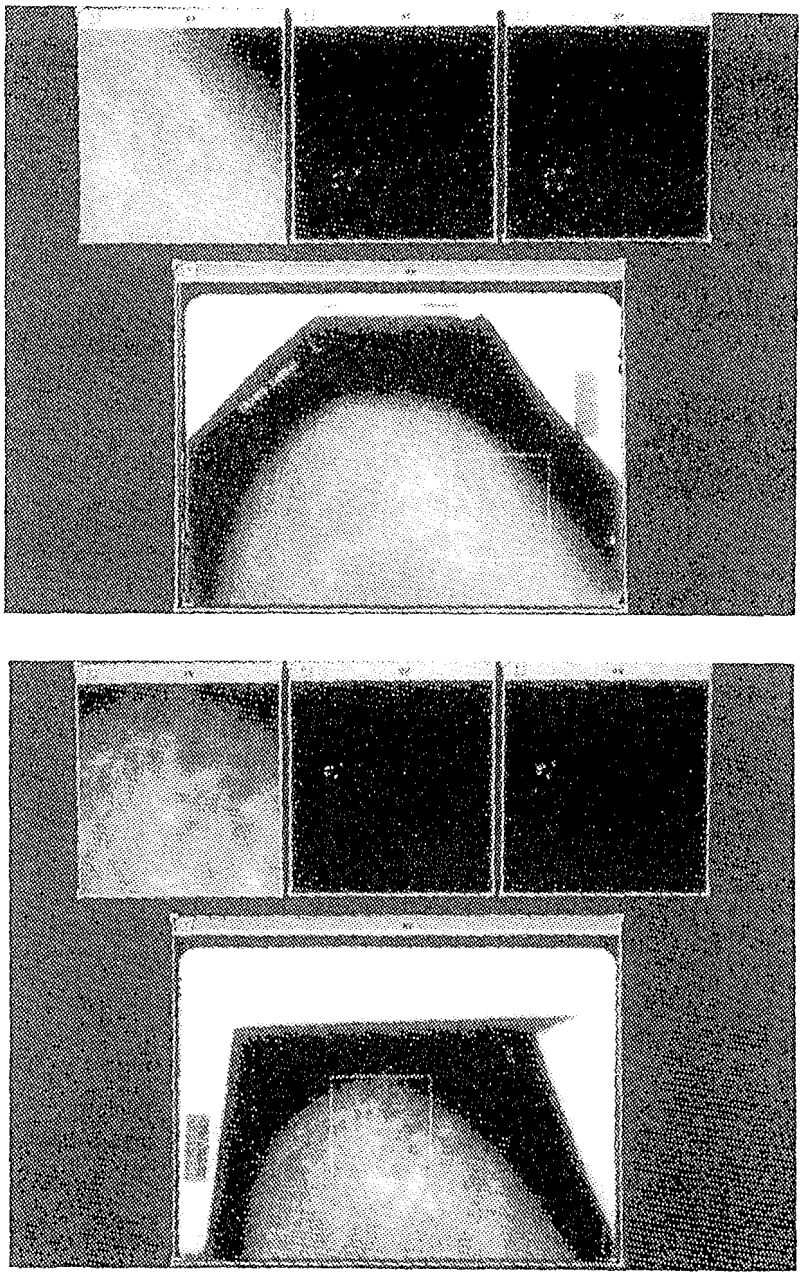

Figure 5.2: Two examples of superimposed synthetic microcalcifications on normal mammograms. The regions where the objects were superimposed are shown enlarged, together with the truth images and the segmentation results (left to right).

It should be noted that in cases where no microcalcifications were detected, careful examination on pixel level shows no presence of visible small bright objects.

The second set of mammograms consisted of 10 images digitized at resolution of .1 mm. In order to achieve required resolution the mammograms were digitized in parts. Each digitized mammogram was verified by the medical expert to contain both macrocalcifications and microcalcifications. The diameter of macrocalcifications varied from 4 to 6 pixels (area varied $12 - 25$ pixels); the diameter of microcalcifications was $1 - 2$ pixels (area varied $1 - 3$ pixels). The results are as follows:

- The presence of macrocalcifications was correctly detected in all cases.
- The presence of some microcalcifications was detected in all cases.
- An average of 2 false positives (2 pixels) were detected in cases when microcalcifications are present in an image.
- Up to 50% of individual microcalcifications were missed if
  - contrast, relative to the neighboring pixels, was below 15
  - an individual microcalcification was adjacent to a small dark region on only one of its sides.

It should be noted that the contrast of 15 between microcalcifications and the neighboring pixels is in agreement with findings for synthetic images. A bright pixel neighboring with an individual dark pixel is perceived as a gray region at lower resolution. If the mean of this region is close to the mean of the larger neighborhood, the bright pixel, i.e., the microcalcification, may be missed. In summary, the method detects all calcifications of area larger than 2 pixels, and about 50% of the smaller calcifications. Also, the method detects no false positives in images where no

microcalcifications are present. Examples of detected microcalcifications are shown in Figure 5.3.

5.3 Detection of Nodules

As in the case of microcalcifications, we have performed two sets of experiments using synthetic objects superimposed on normal mammograms and mammograms containing irregular masses. The results are summarized in the following.

Synthetic Nodules

These experiments consisted in changing the shape, size, and contrast of objects superimposed on normal mammograms in order to establish the sensitivity of the proposed method. Generally, the method can tolerate significant variations of either size or contrast. When the contrast dropped to 10 (relative to the region mean) in cases of the average local standard deviation of 9.5 or when the minor axis dropped below 10 in the same cases, the method has failed to accurately extract objects. (The segmentation started from the level of size 8×8.) Further decrease of either contrast to 8 or minor axis to 9 has resulted in the method's lack of ability to detect objects of interest.

Also, the method has shown sensitivity to shape, and in cases of star-like objects its accuracy was lower than in the case of round objects. However, the method has failed for the same contrasts. (The size experiments do not apply to this case due to the nature of the object.)

Real Nodules

A total of 12 images, supplied by the University of South Florida and labelled irregular mass, were available for this study. The results are as follows:

- In 8 cases the method has detected nodules in agreement with the truth images.

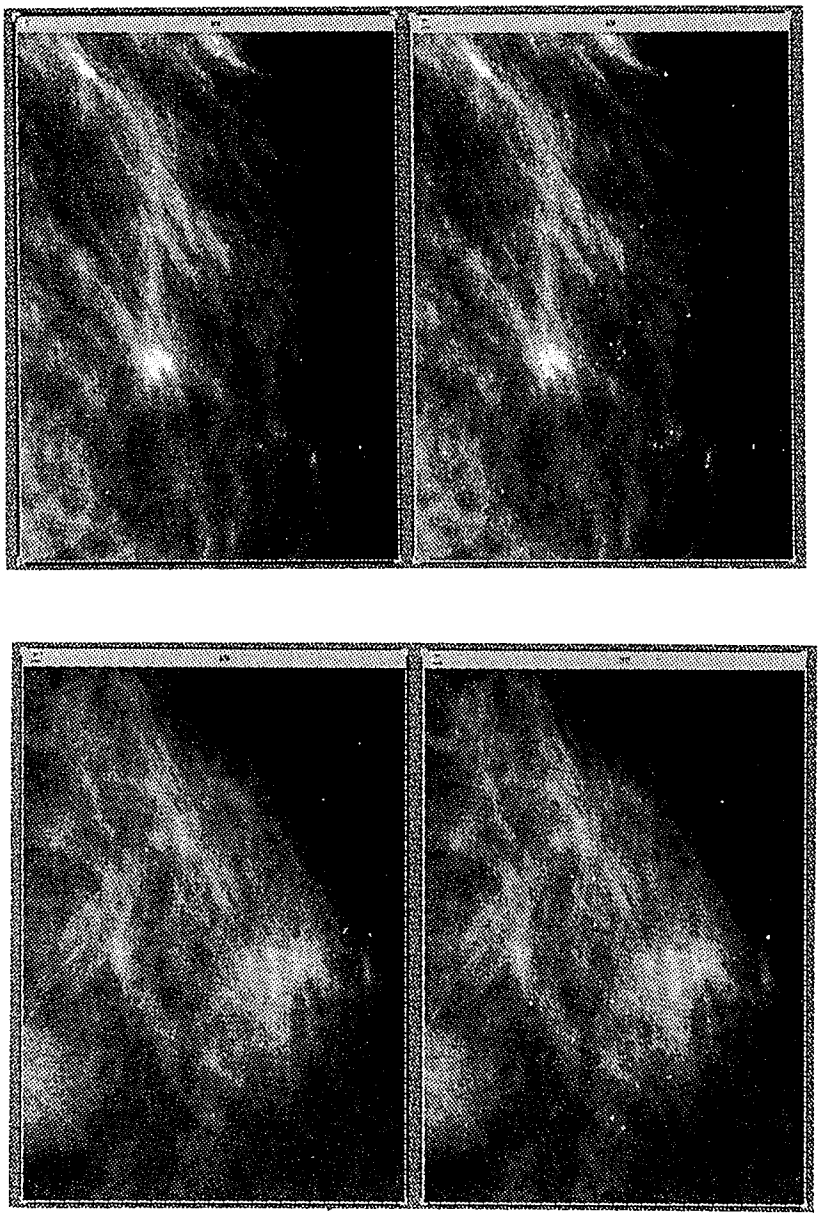

Figure 5.3: Two examples of mammograms containing microcalcifications. The original image is shown on the left, and the detected microcalcifications are shown enhanced on the right.

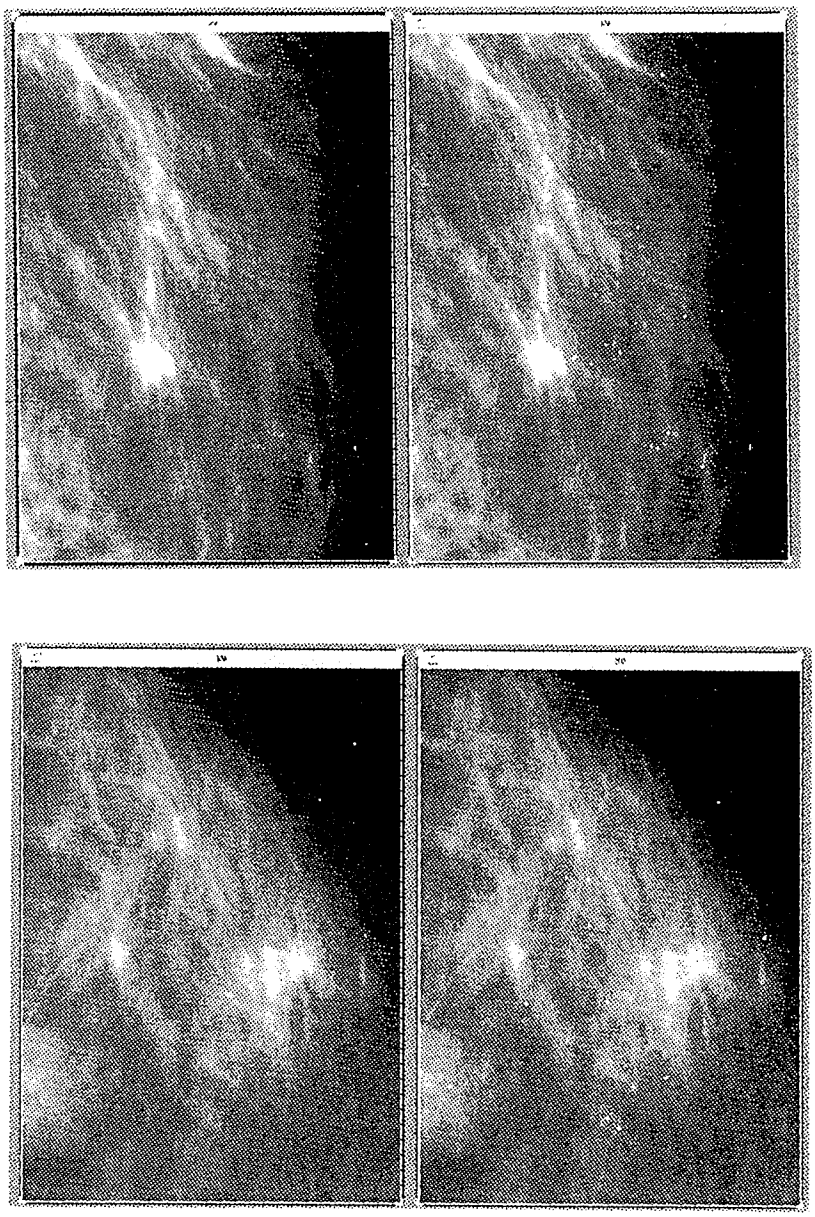

Figure 5.3: Two examples of mammograms containing microcalcifications. The original image is shown on the left, and the detected microcalcifications are shown enhanced on the right.

Except for the edge location, the agreement is on pixel to pixel basis.

- Regarding the edge location, there is an average disagreement for up to ± 3 pixels per object.
- In the remaining 4 mammograms the method has detected only the rudiments of the nodules, and more than 50% of object's pixels were missed.
- The method has detected false positives in 5 out of 50 normal mammograms.

The incidence of false positives can be reduced by post-processing that examines the shape and intensity characteristics of the extracted objects. Examples of two detected nodules, the corresponding truth images, and the obtained results are shown in Figure 5.4.

5.4 Advantages of the Proposed Method

Mammograms vary in density and complexity of texture background and therefore require adaptive image processing methods. The proposed method shows unique capability to detect objects that vary in size, shape and contrast. This is best illustrated by the fact that the same method can be adapted for detection of both microcalcifications and nodules. The method is proven to be a generalization of the standard linking methods. In general, it outperforms the hard-linking methods when the objects of interest do not have clearly defined boundaries [8], [23]. It is adaptive and its sensitivity (with respect to intensity/texture variations and object size) depends on the choice of the fuzzy linking function parameters and the choice of the threshold value that allows replacement of a pixel value by the pixel value

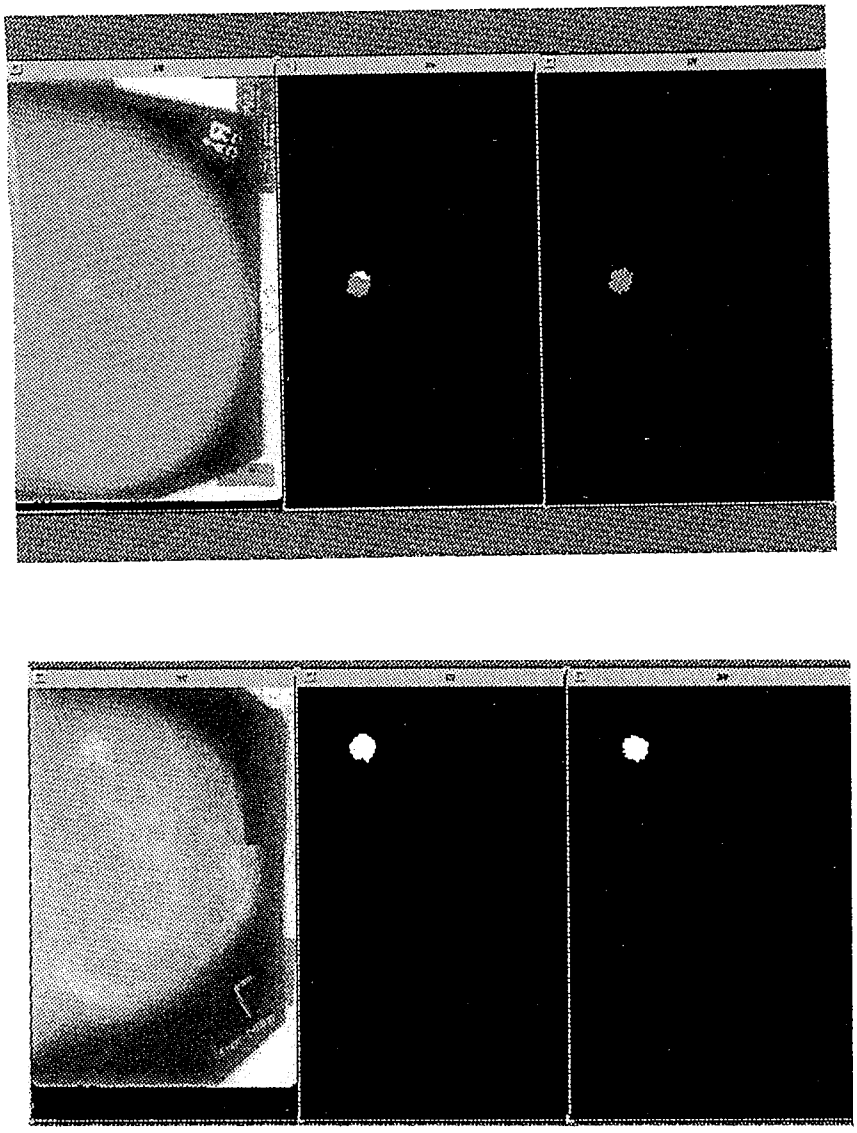

Figure 5.4: Two examples of mammograms containing irregular masses. From left to right: mammogram, truth image, and segmentation results. The top images contains the results obtained by combining outputs of the detected microcalcifications and nodules, since this mammogram contains both (as shown by the truth image).

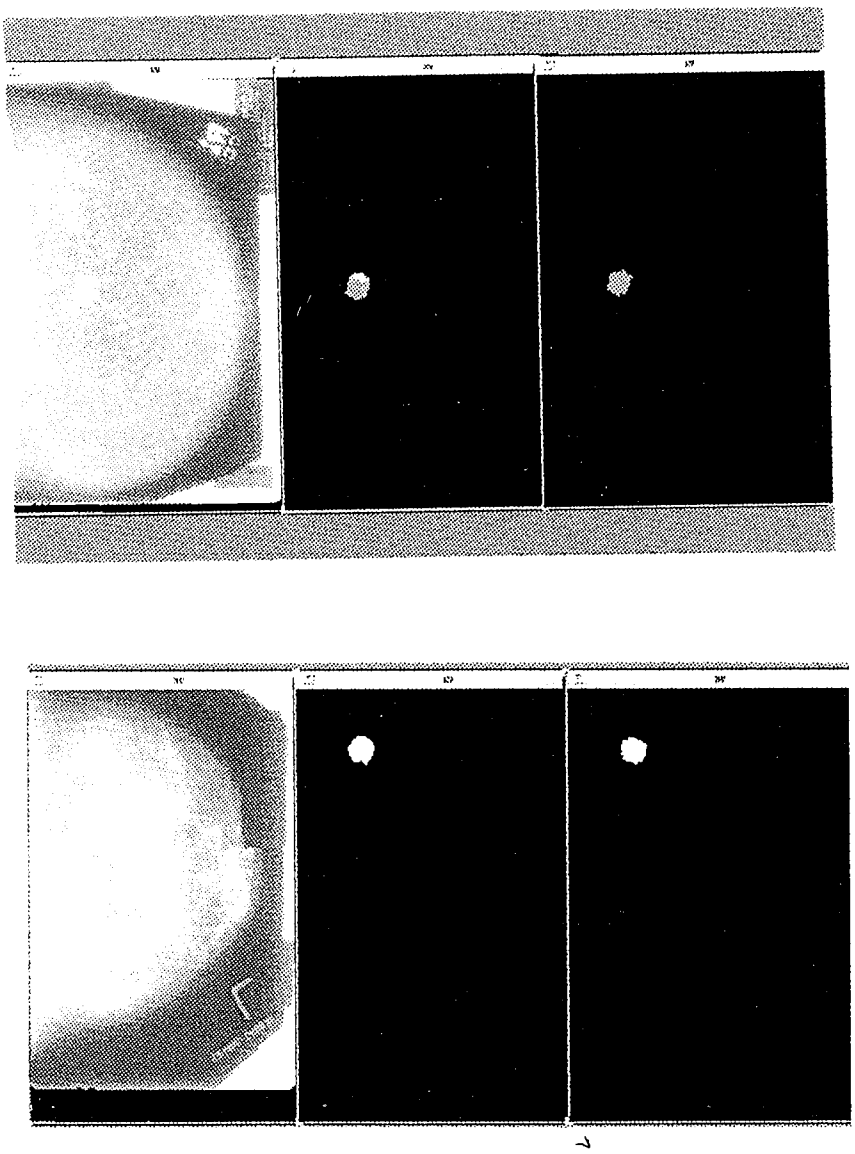

Figure 5.4: Two examples of mammograms containing irregular masses. From left to right: mammogram, truth image, and segmentation results. The top images contains the results obtained by combining outputs of the detected microcalcifications and nodules, since this mammogram contains both (as shown by the truth image).

above. However, the relationship between parameters and performance is robust, and a chosen set of parameter guarantees particular level of performance.

We have compared the performance of the proposed method to gray scale morphology [29] when detecting microcalcifications. The fuzzy pyramid linking yields in general much lower rate of false positives, and in particular it does not detect false positives in mammograms when no microcalcifications are present, in contrast to morphological operators.

The most important advantage of the proposed method lies in the fact that the parameters can be chosen to detect desired contrast and object size. Furthermore, the parameters can be automatically adjusted to texture background. It is possible to combine the outputs obtained with different parameters and assign confidence to the final results based on the changes induced by different parameters of the fuzzy linking function. When varying only the segmentation parameters, the pyramid needs to be generated only once, and the therefore the number of required computations is small.

Chapter 6

Conclusions

In this thesis multiresolution pyramid–based image segmentation was considered. The fuzzy–pyramid linking algorithm was used for hierarchical image representation and segmentation. The relationship between pixels at different pyramid levels was modeled by the fuzzy–membership function. Changing the parameters of this function allows for fine–tuning the method to specific characteristics of images being processed.

The algorithm was tested on mammographic images with objectives: (i) to detect nodules (objects of low contrasts that vary in shape and size) and (ii) microcalcifications (very small objects of somewhat higher contrast). For that purpose two versions of the algorithm were developed. The two versions were evaluated in two ways: (i) using synthetically generated objects superimposed on normal mammograms, and (ii) using mammogram images containing real microcalcifications and nodules. Using synthetically generated objects we were able to precisely determine parameters for the fuzzy membership function and the level from which pyramid linking should start. It gave us useful information of method's capabilities and its sensitivity to object size, shape, and contrast. In all cases the synthetic objects

were detected when contrast difference between the objects and the background was greater than 15 [6]. The real mammograms tests were carried out on 89 images, 60% of which represented normal cases, 25% contained microcalcifications and macrocalcifications, and the remaining 15% contained nodules. All macrocalcifications were correctly detected and 75% of microcalcifications were correctly labeled as suspicious. The algorithm found the presence of nodules in 65% of the cases. The rate of false positives was 10%. It should be noted that the rate of false positives can be reduced by post–processing that takes into consideration shape, dimension and intensity characteristics of the extracted objects.

Preliminary results from the tests show potential in helping the medical experts in early cancer detection. Presently, the method is extended to hierarchical region splitting with objective to provide regions appropriate for comparison in mammogram follow–up [30].

Bibliography

[1] C. Boring, T. Squires, and T. Tong, "Cancer statistics 1991," *Cancer Journal for Clinicians*, vol. 41, pp. 19–51, 1991.

[2] A. Holleb, "Breast cancer: Change and challenge," *CA Cancer Journal for Clinicians*, vol. 41, pp. 69–70, 1991.

[3] M. Morra and B. Blumberg, "Women's perceptions of early detection of breast cancer: How are we doing?," *Seminars in Oncology Nursing*, vol. 7, pp. 151–160, 1991.

[4] B. D. Stewart, D. Folkes, A. Cairns, and I. Ricketts, "Computer image processing in mammographic screening: A review," *Automedica*, vol. 15, pp. 23–45, 1992.

[5] E. Sickles, "Mammographic detectability of breast micro-calcifications," *American Journal of Roentgenology*, vol. 139, pp. 913–918, 1982.

[6] D.Brzakovic and M. Neskovic, "Mammogram screening using multiresolution based image segmentation," *Int. Jour. of Pattern Recognition and Artificial Intelligence*, vol. 7, pp. 1437–1460, 1993.

[7] D. Brzakovic, P. Brzakovic, and M. Neskovic, "Approch to automated screening of mammograms," *Biomedical Image Processing and Biomedic. Visualization - Proc. of IST/SPIE*, vol. 1905, pp. 690–701, 1993.

[8] D. Brzakovic, H. Beck, and N. Sufi, "An approach to defect detection in materials characterized by complex textures," *Pattern Recognition*, vol. 23, pp. 99–107, 1990.

[9] D. Brzakovic, X. Lou, and P. Brzakovic, "An approach to automated detection of tumours in mammograms," *IEEE Transaction on Medical Imaging*, vol. 9, pp. 233–241, 1990.

[10] F. Winsberg, M. Elkin, J. Macy, and V. Bordaz, "Detection of radiographic abnormalities in mmamography by means of optical scaning and computer analysis," *Radiology*, vol. 89, pp. 211–215, 1967.

[11] L. Ackerman, A. Mucciardi, E. Gose, and F. Alcorn, "Classification of benign and malignant breast tumours on the basis of 36 radiographic properties," *Cancer*, vol. 31, pp. 342–352, 1973.

[12] C. Kimme, B. O'Loughlin, and J. Slasky, "Automatic detection of suspicious abnormalities in breast radiographs," in *Data strutcures, Computer Graphics and Pattern Recognition*, New York, NY: Academic Press, 1975.

[13] W. Hand, J. Semmlow, L. Ackerman, and F. Alcorn, "Computer screening of xeromammograms: a technique for defining suspicious areas of the breast," *Computers and Biomedical Research*, vol. 12, pp. 445–460, 1979.

[14] J. Semmlow, A. Shadagopappan, L. Ackerman, and W. Hand, "A fully automatic system for screening mammograms," *Computers and Biomedical Research*, vol. 13, pp. 350–362, 1980.

[15] A. Gale, E. Roebuck, P. Riley, and B. Worthington, "Computer aids to mammographic diagnosis," *British Journal of Radiology*, vol. 60, pp. 887–891, 1987.

[16] A. Hoyer and W. Spiesberger, "Computerized mammogram processing," *Phillips Technical Review*, vol. 38, pp. 347–355, 1979.

[17] H. Chan, K. Doi, S. Galhotra, and C. Vyborny, "Image feature analysis and computer aided diagnosis in digital radiology: automated detection of microcalcifications in mammography," *Medical Physics*, vol. 14, pp. 538–548, 1987.

[18] S. Olsen, B. Fam, P.F.Winter, and F. Scholz, "Breast calcifications: analysis of imaging properties," *radiology*, vol. 169, pp. 329–332, 1988.

[19] I. Bankman, W. Christens-Barry, and I. W. D.W. Kim, "Automated recognition of microcalcification clusters in mammograms," *Procedings of SPIE, Biomedical Image Processing and Biomedical Visualization*, vol. 1905, pp. 731–738, 1993.

[20] P. Burt and E. Andersen, "The laplacian pyramid as a compact image code," *IEEE Trans. on Communication*, vol. 31, pp. 532–540, 1983.

[21] H. Antonisse, "Image segmentation in pyramids," *Computer Graphics and Image Processing*, vol. 19, pp. 367–383, 1982.

[22] P. Burt, "Fast filter transforms for image processing," *Computer Graphics and Image Processing*, vol. 16, 1981.

[23] N. Sufi, "Pyramid based segmentation of texture images," Master's thesis, University of Tennessee, 1988.

[24] L. Zadeh, "Fuzzy sets," *Information and Control*, vol. 8, pp. 338–353, 1965.

[25] J. Bezdek, "A convergence theorem for fuzzy isodata clustering algorithm," *IEEE Trans. on Pattern Analysis and Machine Intelligence*, vol. 2, pp. 1–8, 1980.

[26] S. Kasif and A. Rosenfeld, "Pyramid linking is a special case of isodata," *IEEE Trans. on Systems, Man, and Cybernetics*, vol. 13, pp. 84–85, 1983.

[27] N. Otsu, "A threshold selection method from gray-level histograms," *IEEE Trans. on System, Man and Cybernetics*, vol. 9, pp. 62–66, 1992.

[28] J. Lamarque, *An Atlas of the Breast Clinical Radiodiagnosis.* London, England: Wolfe Medical Publications Ltd., 1981.

[29] S. Sternberg, "Grayscale morphology," *Computer Vision, Graphics and Image Processing*, vol. 35, pp. 333–355, 1986.

[30] D. Brzakovic, N. Vujovic, M. Neskovic, P. Brzakovic, and K. Fogarty, "Mammogram analysis by comparison with previous screenings," *Digital Mammography*, vol. 1069, pp. 131–142, 1994.

END OF TITLE